Similarity Solution of the Partial Differential Equations that model water/magnetite nanofluid flow and heat transfer on a stretchable rotating disk subject to thermal radiation and Lorentz force

Usman, U.; Lin, Ping; Ghaffari, Abuzar; Mustafa, Irfan

Published in:
Numerical Methods for Partial Differential Equations

DOI:
10.1002/num.22677

Publication date:
2020

Document Version
Peer reviewed version

Similarity Solution of the Partial Differential Equations that model water/magnetite nanofluid flow and heat transfer on stretchable rotating disk subject to thermal radiation and Lorentz force

Usman[1*], Ping Lin[2†], Abuzar Ghaffari[3], Irfan Mustafa[4]

[1]Beijing Key Laboratory for Magneto-Photoelectrical Composite and Interface Science, Department of Applied Mathematics, School of Mathematics and Physics, University of Science and Technology Beijing, Beijing 100083, China

[2]Division of Mathematics, University of Dundee, Dundee, DD1 4HN, Scotland, United Kingdom

[3]Department of Mathematics, University of Education, Lahore (Attock Campus), Attock 43600, Pakistan

[4]Department of Mathematics, Allama Iqbal Open University, H-8, Islamabad 44000, Pakistan

Abstract

Among other non-Newtonian fluid models, power-law fluid has gained much acceptance because of its some powerful applications such as pressure drop calculation in the drilling industry, utilization of blood flow for red cells in plasma and static as well as dynamic filtration. The aim is to analyze theoretically the steady three-dimensional boundary layer flow near the stagnation point and heat transfer of power-law ferrofluid over rotatory stretchable. The effect of Lorentz force on the flow and the influence of nonlinear thermal radiation upon the temperature is also incorporated. For this phenomenon, magnetite (Fe_3O_4) is considered as ferrofluid particles which are mixed with the base fluid (water). Physically modeled partial differential equations (PDEs) are lessened to ordinary differential equations (ODEs) by the support of precise similarity transformation and then the shooting method is implemented to obtain the solution of the resultant ODEs. A comprehensive tabular comparison between present and previously existing outcomes is made. From an overall exploration it can be concluded that the cross-sectional flow for shear thinning and shear thickening is examined upon increasing the concentration of the nanoparticles and flow behaving index of power-law. The Lorentz force retards the flow near the disk due to which velocity components decrease. Also, the temperature escalates for nonlinear radiation and this escalation is more prominent for shear thinning. Furthermore, the Prandtl number helps in controlling the boundary layer thickness.

Keywords: Power-law fluid, nonlinear radiation, stagnation point boundary layer flow, Lorentz force, ferrofluid, stretching and rotating disk, shooting method.

List of symbols and their description

$r,\ \theta^*, z$	Cylindrical coordinates	k^*	Mean absorption coefficient
u, v, w	Components of the velocity in $r,\ \theta^*$ and z directions	ϕ	Volume fraction
F, G, H	The dimensionless components of the velocity in radial, azimuthal and axial directions	μ	Dynamic viscosity

* Corresponding author. Usman.
e-mail address: usman.malik.ms@gmail.com
† Corresponding author. Ping Lin.
e-mail address: p.lin@dundee.ac.uk

q_r	Radiative heat flux	Ω	Angular velocity
T_w, T_∞	Uniform surface temperature and ambient fluid temperature	η	Dimensionless similarity variable
$C_{Fr}, C_{G\theta^*}$	Coefficients of skin friction	v	Kinematic viscosity
k	Thermal conductivity	θ	Dimensionless temperature
M	Magnetic parameter	λ	Velocity ratio parameter
Nu_r	Local Nusselt number	σ^*	Stefan-Boltzmann constant
Re_r	Local Reynolds number	Pr	Prandtl number
u_e, v_e	Free stream velocities	θ_w	Temperature ratio
B_0	Uniform magnetic field	ω	Rotation parameter
T	Fluid temperature	$\tau_{rz}, \tau_{G\theta^*}$	Radial and azimuthal shear stresses
c_p	Specific heat at constant pressure	ρ	Density of fluid
n	Power-law index		
Rd	Radiation parameter	**Subscripts**	
q_w	Constant heat flux	nf	Nanofluid
B_1, B_2, B_3, B_4, B_5	Constant parameters	f	Base fluid
σ	Electrical conductivity	s	Ferrofluid

1. Introduction

In the past decade, the nanofluid has been widely studied by several researchers because of its numerous industrial applications. The word nanofluid was initially used by Choi [1]. Many solid particles more precisely metals have higher effects of thermal conductivity with the comparison of base fluids, for instance, oil, water, and ethylene with a mixture of glycol, which are relatively having a lower effect of thermal conductivity and they termed as poor heat transfer fluids. To enhance the thermal conductivity of such base fluids, solid particles of the nano-sized having a length of 100 nm are commonly attached to them called nanofluid. Many researchers have investigated the heat transfer in nanofluid, for instance, Abu Nada [2], Tiwari and Das [3], and Jaluria et al. [4]. The greatest pressure, greatest heat, and mass transfer rates can be found in the stagnation point region. Bachok et al. [5] was the first one who has considered the heat transfer with the occurrence of nanofluid and by considering three-dimensional stagnation point flow. They assumed Copper, Alumina, and Titania as three nano-particles and found out that copper water-based nanofluid under the circumstances of assisting flow has a higher rate of heat transfer. Babu and Sandeep [6] have considered the three-dimensional MHD slip flow of nanofluid and performed the theoretical analysis to investigate the convective heat and mass transfer upon a slandering sheet which is stretching. They have assumed the water and graphene as well as magnetite as a base fluid and nanoparticles and concluded that the heat and mass transfer rates are higher water-graphene nanofluid than from water-magnetite nanofluid. Mustafa et al. [7] explored the heat transfer with the occurrence of nonlinear thermal radiation for the MHD three-dimensional rotating flow of magnetite-water nanofluid. They have reflected a novel idea of nonlinear radiative heat flux due to which nonlinear energy equation in the temperature field is produced. Anu and Hemalatha [8] synthesized water-based magnetite nanofluids of different

concentrations via the co-precipitation method by studying the density and viscosity of different concentrations for ferrofluids at room temperature. Amini et al. [9] studied the MHD flow of magnetite-water nanofluid and heat transfer inside the porous medium alongside a flat sheet with the effects of the chemical reaction. Hayat et al. [10] presented a communication that deals with the influence of homogeneous-heterogeneous reactions in the flow which is composed of water-based nanofluid containing magnetite nanoparticles. Bhatti et al. [11] numerically studied the effects of the slip flow and thermal radiation upon the magnetic water-based nanofluid over nonlinearly stretching sheet inside the porous media. Later on, the nanofluid has been considered and explored by some other researchers in [12-14].

Flow and heat transfer in the vicinity of disk rotation is one of the most prominent parts of the research studies and particular interests due to its enormous usage in engineering for example lubrication, turbine system, rotating parts of electrical devices. The examination of fluid flow motion over an infinitely rotating disk was originally debated by von Karman [15] who proposed the generalized similarity transformations due to which PDEs are switched to ODEs and handled them with the help a method named as momentum integral. But the concept of fluid flow because of disk rotation has taken a long time to accomplish its significance [16-18]. Irfan Mustafa et al. [19] has studies the heat transfer in stagnation point MHD ferrofluid over a rotatory stretchable disk by choosing three ferrofluid particles namely magnetite, cobalt ferrite, Mn-Zn ferrite. A non-Newtonian fluid is a type of fluid that is based upon applied stress and having variable viscosity. The non-Newtonian fluids which obey the properties of shear-thinning and shear-thickening are known as power-law fluids. Mitschka [20] enhanced the transformation of von Karman to a power-law fluid. Mitschka and Ulbricht [21] have numerically obtained the results for disk rotation flow by shear dependent viscosity within the limit $0.2 \leq n \leq 1.5$ of the power-law index. Andersson et al. [22] re-consider the study of Mitschka and Ulbricht [21] and comprehended that the boundary layer thickness is increasing with the decrease in the power-law index n from 2 to 0.2. Andersson and Korte [23] further succeeded in applying the MHD on power-law fluid and determined that shear-thinning has more influence on the magnetic field than shear-thickening. Lian-Cun et al. [24] has studied the power-law fluid and investigated the fully developed convective heat transfer in the vicinity of the circular tube with the assumption that thermal diffusivity is a function of the temperature gradient. Ming et al. [25] further explored the power-law fluid for steady flow and heat transfer over a rotatory disk with the assumption that the viscosity and thermal conductivity fulfill the similar properties of power-law In 2019 Nabil T. El-Dabe et al. [26] scrutinized the steady power-law MHD nanofluid flow due to uniformly rotating infinite disk. Usman et al. [27] made a valuable contribution to exploring the power-law fluid between two rotatory stretchable disks. Some worth mentioning researches on the fluid flow upon disk geometry are deliberated in [28-31].

Radiation is extremely effective in material, mechanical, and engineering science due to its several promising applications such as polymer preparation, glass generation, furnace design, and gas-cooled atomic reactors. It is further applicable in space innovation for the instance propulsion system, rockets and space craft's operating at high temperature. The radiation which is transmitted by a body is because of the thermal agitation of particles it produces. Several researchers [32-37] have investigated the effects of thermal radiation upon utilizing the linearized form of the Rosseland flow. However, the linear radiation is not applicable for higher temperature difference as the dimensionless parameter which is involved in the linearization of the Rosseland flow is just the effective Prandtl number [38]. In the case of nonlinear radiation three parameters namely, Prandtl number, radiation parameter, and temperature ratio parameter are usually used to govern the problem. The nonlinear radiation is effective for a small and large temperature

difference of surface and ambient fluid. Researchers like Sravanthi [39], Waqas et al. [40], and Mkhatshwa et al. [41] made valuable contributions in exploring the effects of increasing nonlinear thermal radiation in diverse modes.

With the occurrence of a magnetic field, the motion of an electrically conducting fluid is known as magnetohydrodynamics (MHD). Alfven [42] stated that when we place an electrically conducting liquid within a constant magnetic field, the movement of these liquids yields the electromotive force which generates the electric currents. A type of electromotive force induces current whereas another one trends to produce the Lorentz force. It is further observed that due to the magnetic field, these currents provide mechanical forces that modify the liquid's state of motion. Ever since, its application has been reported by the researchers in metallurgy, MHD generators, MHD designed pumps, fusion reactors, and MHD flow meters. Makinde et al. [43] has numerically explored the heat transfer with the effects of Lorentz force upon the MHD flow of Casson fluid over a thermally stratified melting surface. Animasaun et al. [44] presented the influence of applied magnetic field and Hall effects upon the flow which is produced from 29nm CuO-water nanofluid. Koriko et al. [45] presented the comparative study by considering the three-dimensional flow of nanofluid inside the thin boundary layer upon a bidirectional surface which is stretching linearly. Mahanthesh et al. [46] has investigated the nanofluid flow close to radially stretching disk with the occurrence of exponential space-based and thermal-based heat sources by deploying the effects of Coriolis and Lorentz forces. Li et al. [47] studied the influence of Lorentz force and anisotropic thermal conductivity concerning the magnetic field upon the flow and heat transfer of Ferro-nanofluid. Wakif et al. [48-49] has numerically examined the electrically conducting fluid over the plate geometry.

After thoroughly gone through the literature, some studies exist on ferrofluid due to the rotatory disk. Researchers like Ram at el. [50-52] and Hayat et al. [53] investigated the ferrofluid with a rotating disk. Later on, Ram and Sharma [54-55] and Hassan et al. [56] evaluated the influence of rotation and stretching of MHD ferrofluid with the analysis of disk rotation respectively. But the nonlinear thermally radiated MHD stagnation point boundary layer flow of a power-law ferrofluid upon a rotatory stretchable disk is not demonstrated until now. So the goal of the current research article is to find the similarity solution of the PDEs that models from water/magnetite nanofluid flow on a stretchable rotatory disk subject to nonlinear thermal radiation and Lorentz force. The modeled nonlinear PDEs of motion and energy in the specified boundary layer are numerically tackled through the shooting method. The parametrical influence of non-Newtonian power-law fluid accentuated and full parametrical study is conducted.

The graphical illustration and tables are typical answers to some unknown questions. This is true because the current theoretical analysis has comprehensively addressed the worth mentioning answers to some interesting research questions. Therefore, the following questions may help the readers to link what is known in the literature with the novelty of the current study:

1. What are the effects of volume fraction parameter, the magnetic field parameter, the rotation parameter, power-law index, temperature ratio parameter, radiation parameter and Prandtl number upon the dimensionless distributions of velocity and temperature?
2. In which situation problem the effects of MHD and nonlinear thermal radiation can be utilized in the momentum and energy equations for steady three dimensional stagnation point flow?
3. What are the suitable expressions of dynamic viscosity and thermal conductivity when they follow the power-law characteristics?

4. How we can apply the shooting method that is used to obtain the similarity solution of the partial differential equations that model water/magnetite nanofluid flow and heat transfer on stretchable rotating disk subject to thermal radiation and Lorentz force?
5. How the stretchable rotatory disk is advantageous upon the skin friction factor and heat transfer rate?

2. Physical model and formulation of the problem

The three-dimensional incompressible stagnation point flow of power-law with the aim of ferrofluid on a rotatory stretchable disk is taken into consideration as displayed in Fig. 1. The assumed flow is steady and axisymmetric. The components of velocity (u, v, w) along with the cylindrical coordinate system (r, θ^*, z) are chosen. The rotation of disk concerning constant angular velocity Ω along z-axis has been assumed. The disk by a constant rate c and with the velocity $u = cr$ is stretching in the radial direction. The variation due to θ^* is vanished because of the axisymmetric flow behavior. The externally operated uniform magnetic field which is maintaining the strength of B_0 is applied perpendicularly along the z-axis to the circulating disk. Thus, the ferrofluid becomes magnetized strongly it is because ferrofluids without outwardly performing magnetic field are unable to retain the effects of magnetization. The inducible magnetic field is treated as negligible by the hypothesis of Reynolds number having small magnetic effects. The gradient of pressure $(\partial p/\partial z = 0)$ is vanished in the z-direction with the help of derivation of the boundary layer which is proposed by Andersson et al. [22]. Also, Karman's similarity transformation implies that $(\partial p/\partial r = 0)$, which means the pressure is treated as constant throughout the boundary layer. Furthermore, the velocity which is exterior to the boundary layer can be specified as a potential flow that is $u_e = ar$. The constant temperature T_w is kept at the surface of the disk rotation and the fluid which is flowing outside of the boundary layer is placed at an ambient uniform temperature T_∞ with $T_w > T_\infty$.

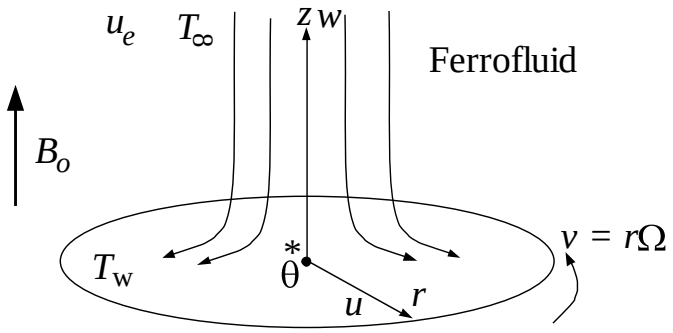

Fig 1. The flow geometry of power-law fluid towards the disk rotation about the stagnation point zone.

Table 1

The thermophysical properties of the particles of the base fluid and ferrofluid [19].

Properties	Water	Fe_3O_4
$c_p(J/KgK$	4179	670
$\rho(Kg/m^3$	997.1	5180
$\kappa(W/mK)$	0.613	9.7
$\sigma(S/m)$	0.05	2.5×10^3

Table 1 illustrates the thermophysical properties of pure water as a base fluid and Ferrite Fe_3O_4 as a ferrofluid particle. The governing continuity, momentum, and energy equations within the boundary layer of the proposed problem in the form of cylindrical co-ordinates can respectively be expressed as [27]

$$\frac{\partial u}{\partial r}+\frac{u}{r}+\frac{\partial w}{\partial z}=0 \tag{1}$$

$$u\frac{\partial u}{\partial r}-\frac{v^2}{r}+w\frac{\partial u}{\partial z}=u_e\frac{du_e}{dr}+\frac{1}{\rho_{nf}}\frac{\partial}{\partial z}\left(\mu\frac{\partial u}{\partial z}\right)-\frac{\sigma_{nf}B_0^2}{\rho_{nf}}\left(u-u_e\right) \tag{2}$$

$$u\frac{\partial v}{\partial r}+\frac{uv}{r}+w\frac{\partial v}{\partial z}=\frac{1}{\rho_{nf}}\frac{\partial}{\partial z}\left(\mu\frac{\partial v}{\partial z}\right)-\frac{\sigma_{nf}B_0^2}{\rho_{nf}}v \tag{3}$$

$$u\frac{\partial T}{\partial r}+w\frac{\partial T}{\partial z}=\frac{1}{\left(\rho c_p\right)_{nf}}\left\{\frac{\partial}{\partial z}\left(\kappa\frac{\partial T}{\partial z}\right)-\frac{\partial q_r}{\partial z}\right\} \tag{4}$$

Where (u,v,w) denotes the components of the velocity alongside cylindrical co-ordinates (r,θ^*,z), u_e be the free stream velocity, ρ_{nf} is the effective density and σ_{nf} be an electrical conductivity of the nanofluid, B_0 is said to be the force of the uniformly applied magnetic field, $\left(\rho c_p\right)_{nf}$ stated as the specific heat at the constant rate of the pressure of the nanofluid.

Lian-Cun et al. [24] has chosen the dynamic viscosity μ and thermal conductivity k as follows:

$$\mu=K\left[\frac{\partial u}{\partial r}\right]^{n-1},\ k=K\left[\frac{\partial T}{\partial r}\right]^{n-1} \tag{5}$$

In which K is the positive constant.

Ming et al. [25] assumed the dynamic viscosity μ and thermal conductivity k are of the following types:

$$\mu=\mu_0\left\{\left(\frac{\partial u}{\partial z}\right)^2+\left(\frac{\partial v}{\partial z}\right)^2\right\}^{(n-1)/2},\ \kappa=\kappa_0\left\{\left(\frac{\partial u}{\partial z}\right)^2+\left(\frac{\partial v}{\partial z}\right)^2\right\}^{(n-1)/2} \tag{6}$$

Where μ_0 and k_0 are the constants.

Upon utilizing [24-25] the dynamic viscosity μ and thermal conductivity k in the presence of nanofluid particles are delineated as:

$$\mu = \mu_{nf}\left\{\left(\frac{\partial u}{\partial z}\right)^2 + \left(\frac{\partial v}{\partial z}\right)^2\right\}^{(n-1)/2}, \ \kappa = \kappa_{nf}\left\{\left(\frac{\partial u}{\partial z}\right)^2 + \left(\frac{\partial v}{\partial z}\right)^2\right\}^{(n-1)/2} \tag{7}$$

In which μ_{nf} indicates the dynamic viscosity, k_{nf} denotes the thermal conductivity and T represents the temperature of the nanofluid respectively and n shows the power-law index.

The simplified form for radiative heat flux in terms of approximation of Rosseland can be stated as

$$q_r = -\frac{4\sigma^*}{3k^*}\frac{\partial T^4}{\partial z} = -\frac{16\sigma^* T^3}{3k^*}\frac{\partial T}{\partial z}, \tag{8}$$

Where σ^* is the constant of Stefan-Boltzmann and k^* is the coefficient of mean absorption. The relationships for ρ_{nf}, μ_{nf}, σ_{nf}, $(\rho c_p)_{nf}$ and k_{nf} are defined as follows:

The relationships for effective density ρ_{nf} and capacitance of heat of the nanofluid is chosen the same as in [19]:

$$\rho_{nf} = (1-\phi)\rho_f + \phi\rho \tag{9}$$

$$(\rho c_p)_{nf} = (1-\phi)(\rho c_p)_f + \phi(\rho c_p)_s \tag{10}$$

The dynamic viscosity for the nanofluid is taken as [19]

$$\mu_{nf} = \frac{\mu_f}{(1-\phi)^{2.5}} \tag{11}$$

The effective thermal and electrical thermal conductivities of the nanofluid are [19];

$$\frac{k_{nf}}{k_f} = \frac{(k_s + 2k_f) - 2\phi(k_f - k_s)}{(k_s + 2k_f) + \phi(k_f - k_s)} \tag{12}$$

$$\frac{\sigma_{nf}}{\sigma_f} = 1 + \frac{3\left(\frac{\sigma_s}{\sigma_f} - 1\right)\phi}{\left(\frac{\sigma_s}{\sigma_f} + 2\right) - \left(\frac{\sigma_s}{\sigma_f} - 1\right)\phi} \tag{13}$$

Here, μ_f be the dynamic viscosity for base fluid and ϕ elucidates the volume fraction of nanoparticles. The other quantities like ρ_f and ρ_s, σ_f and σ_s, $(\rho c_p)_f$ and $(\rho c_p)_s$, k_f and k_s are the densities, electrical conductivities, specific heats, thermal conductivities of the base, and nanofluid respectively.

The desired boundary conditions for the proposed phenomenon are given by

$$u = cr, \ \ v = \Omega r, \ \ w = 0, \ \ T = T_w, \ \text{ at } \ z = 0, \tag{14}$$

$$u = u_e \to ar, \ \ v = v_e \to 0, \ T = T_\infty, \ \text{ at } \ z = \infty, \tag{15}$$

Introducing the suitable similarity transformation for the present fluid flow problem as follows Usman et al. [27].

$$\begin{aligned}&\eta = z\left(\frac{c^{2-n}}{\nu_f}\right)^{1/(n+1)} r^{(1-n)/(1+n)},\ u = cr.F(\eta),\ v = cr.G(\eta),\\ &w = \left(\frac{c^{1-2n}}{\nu_f}\right)^{-1/(n+1)} r^{(n-1)/(n+1)},\ H(\eta),\ T = T_\infty + (T_w - T_\infty)\theta(\eta).\end{aligned} \tag{16}$$

Upon using (16) into (1-4), the resulting system of ODEs can be written as

$$H' = -2F - \frac{1-n}{1+n}\eta F' \tag{17}$$

$$F^2 - G^2 + \left(H + \frac{1-n}{1+n}\eta F\right)F' = \lambda^2 + \frac{B_2}{B_1}\left\{F'\left[(F')^2 + (G')^2\right]^{(n-1)/2}\right\}' - \frac{B_3}{B_1}M(F-\lambda) \tag{18}$$

$$2FG + \left(H + \frac{1-n}{1+n}\eta F\right)G' = \frac{B_2}{B_1}\left\{G'\left[(F')^2 + (G')^2\right]^{(n-1)/2}\right\}' - \frac{B_3}{B_1}MG \tag{19}$$

$$\left(H + \frac{1-n}{1+n}\eta F\right)\theta' = \frac{B_5}{B_4}\frac{1}{\Pr}\left\{\left[1 + Rd\left(1 + (\theta_w - 1)\theta\right)^3\right]\theta'\left[(F')^2 + (G')^2\right]^{(n-1)/2}\right\}' \tag{20}$$

Where, η is the dimensionless similarity variable, $F, G\ and\ H$ be dimensionless velocity components in radial, azimuthal and axial directions, θ is the dimensionless temperature, $'$ represents the derivative w. r. t. η and ν_f is the base fluid kinematic viscosity.

The other parameters which help the fluid flow to govern can be classified in the following fashion.

$$B_1 = \frac{\rho_{nf}}{\rho_f},\ B_2 = \frac{\mu_{nf}}{\mu_f},\ B_3 = \frac{\sigma_{nf}}{\sigma_f},\ B_4 = \frac{(\rho c_p)_{nf}}{(\rho c_p)_f},\ B_5 = \frac{k_{nf}}{k_f} \tag{21}$$

$$\lambda = \frac{a}{c},\ M = \frac{B_0^2\sigma_f}{\rho_f c},\ \Pr = \frac{(\rho c_p)_f \nu_f}{k_f},\ Rd = \frac{16\sigma^* T_\infty^3}{3kk^*},\ \theta_w = \frac{T_w}{T_\infty} \tag{22}$$

Where $B_1, B_2, B_3, B_4\ and\ B_5$ are the constant parameters, λ is the velocity ratio parameter, M is the magnetic parameter, Pr represents the Prandtl number, Rd is the parameter of the radiation and θ_w indicates the ratio of the temperature.

The reduced boundary conditions are

$$F(0) = 1,\ \ G(0) = \omega,\ \ H(0) = 0,\ \ \theta(0) = 1 \tag{23}$$

$$F(\infty) = \lambda,\ \ G(\infty) = 0,\ \ \ \theta(\infty) = 0, \tag{24}$$

The $\omega = \frac{\Omega}{c}$ here refers to the parameter of rotation.

3. Physical Quantities

3.1 Surface Drag Forces

The surface drag forces or radial and azimuthal directions skin friction coefficients can be expressed with the relations as in [27];

$$C_{Fr} = \frac{\tau_{rz}}{\rho_f (cr)^2},\ C_{G\theta^*} = \frac{\tau_{\theta^* z}}{\rho_f (cr)^2}, \tag{25}$$

The terms here $\tau_{rz}, \tau_{\theta^* z}$ denotes shear stresses in radial and azimuthal directions and q_w is the constant heat flux, these are given by

$$\tau_{rz} = \left[\mu \left\{ \left(\frac{\partial u}{\partial z} \right) + \frac{1}{r} \left(\frac{\partial w}{\partial \theta^*} \right) \right\} \right]_{z=0} = \left[\mu \left(\frac{\partial u}{\partial z} \right) \right]_{z=0},\ \tau_{\theta^* z} = \left[\mu \left\{ \left(\frac{\partial v}{\partial z} \right) + \frac{1}{r} \left(\frac{\partial w}{\partial \theta^*} \right) \right\} \right] = \left[\mu \left(\frac{\partial v}{\partial z} \right) \right]_{z=0}, \tag{26}$$

By using the transformation (16), the (26) will take a new form as

$$\mathrm{Re}_r^{\frac{1}{n+1}} C_{Fr} = A_2 \left[F'^2(0) + G'^2(0) \right]^{\frac{n-1}{2}} F'(0),\ \mathrm{Re}_r^{\frac{1}{n+1}} C_{G\theta^*} = A_2 \left[F'^2(0) + G'^2(0) \right]^{\frac{n-1}{2}} G'(0), \tag{27}$$

3.2 Heat Transfer Rates

The mathematical relation of heat transfer rates or local Nusselt number Nu_r for the present flow is [27]

$$Nu_r = \frac{r q_w}{k(T_W - T_\infty)}, \tag{28}$$

Where, q_w is the heat flux and is given by

$$q_w = \left[-k \frac{\partial T}{\partial z} + (q_r)_w \right]_{z=0} = -\left[\left\{ 1 + Rd \left(1 + (\theta_w - 1)\theta \right)^3 \right\} k \frac{\partial T}{\partial z} \right]_{z=0}. \tag{29}$$

The non-dimensional form is

$$\mathrm{Re}_r^{-\frac{1}{n+1}} Nu_r = -\left[1 + Rd \left(1 + (\theta_w - 1)\theta(0) \right)^3 \right] \theta'(0). \tag{30}$$

In which $Re_r = \frac{r^2 c^{2-n}}{\nu_f}$ be the local Reynolds number.

4. Shooting Method

The numerical technique adopted here is a shooting method for finding the solution of highly nonlinear ODEs (17-20) subject to the boundary conditions (23-24). The solution scheme for the shooting method is based on the following steps.

The proposed BVP w.r.t. boundary conditions can be transformed into the first order IVP by defining the derivatives as

$$y_1 = F,\ y_2 = F',\ y_3 = G,\ y_4 = G',\ y_5 = H,\ y_6 = \theta,\ y_7 = \theta'. \tag{31}$$

This implies that (17-20) reduces to a system of IVP in terms of seven interconnected first-order equations using seven functions i.e. y_N $(N = 1,2,\ldots,7)$.

$$\begin{aligned}
y_1' &= y_2,\\
y_2' &= \frac{1}{n}\left(y_2^2 + y_4^2\right)^{\frac{1-n}{2}} \frac{B_1}{B_2}\left\{\begin{array}{l}\left[1+(n-1)\left(y_2^2+y_4^2\right)^{-1} y_4^2\right]\left[y_1^2 - y_3^2 + \left(y_5 + \frac{1-n}{1+n}\eta y_1\right) y_2 - \lambda^2 + \frac{B_3}{B_1} M\left(y_1 - \lambda\right)\right]\\ -(n-1)\left(y_2^2+y_4^2\right)^{-1} y_2 y_4\left[2y_1 y_3 + \left(y_5 + \frac{1-n}{1+n}\eta y_1\right) y_4 + \frac{B_3}{B_1} M y_3\right]\end{array}\right\},\\
y_3' &= y_4,\\
y_4' &= \frac{1}{n}\left(y_2^2 + y_4^2\right)^{\frac{1-n}{2}} \frac{B_1}{B_2}\left\{\begin{array}{l}\left[1+(n-1)\left(y_2^2+y_4^2\right)^{-1} y_2^2\right]\left[2y_1 y_3 + \left(y_5 + \frac{1-n}{1+n}\eta y_1\right) y_4 + \frac{B_3}{B_1} M y_3\right]\\ -(n-1)\left(y_2^2+y_4^2\right)^{-1} y_2 y_4\left[y_1^2 - y_3^2 + \left(y_5 + \frac{1-n}{1+n}\eta y_1\right) y_2 - \lambda^2 + \frac{B_3}{B_1} M\left(y_1 - \lambda\right)\right]\end{array}\right\},\\
y_5' &= -2y_1 - \frac{1-n}{1+n}\eta y_2,\\
y_6' &= y_7,\\
y_7' &= \frac{y_7}{\left[1+Rd\left(1+\left(\theta_w - 1\right) y_6\right)^3\right]}\left\{\begin{array}{l}\left(y_2^2 + y_4^2\right)^{\frac{1-n}{2}}\left[\begin{array}{l}\left(\frac{B_4}{B_5}\Pr - \frac{B_1}{B_2}\left(1+Rd\left(1+\left(\theta_w-1\right)y_6\right)^3\right)\frac{n-1}{n}\right)\left(y_5 + \frac{1-n}{1+n}\eta y_1\right)\\ -\frac{B_1}{B_2}\left(\left(1+Rd\left(1+\left(\theta_w-1\right)y_6\right)^3\right)\frac{n-1}{n}\left(y_2^2+y_4^2\right)^{-1}\right)\times\\ \left(y_1^2 y_2 - y_2 y_3^2 + 2y_1 y_3 y_4 - \lambda^2 y_2 + \frac{B_3}{B_1} M\left(y_2\left(y_1 - \lambda\right) + y_3 y_4\right)\right)\end{array}\right]\\ -3Rd\left(1+\left(\theta_w - 1\right) y_6\right)^2\left(\theta_w - 1\right) y_7\end{array}\right\}
\end{aligned} \tag{32}$$

The boundary conditions reduce to

$$\begin{gathered}
y_1(0) = 1,\ y_2(0) = a_1,\ y_3(0) = \omega,\ y_4(0) = a_2,\ y_5(0) = 0,\ y_6(0) = 1,\ y_7(0) = a_3,\\
y_1(\infty) = \lambda,\ y_3(\infty) = 0,\ y_6(\infty) = 0.
\end{gathered} \tag{33}$$

Here $y_2(0) = a_1$, $y_4(0) = a_2$ and $y_7(0) = a_3$ are the missing initial conditions that can be obtained subject to $y_1(\infty) = \lambda, y_3(\infty) = 0$ and $y_2(\infty) = 0$ for instance by setting the values of the parameters as $n = Pr = \theta_w = 1, M = 2,\ \lambda = \phi = Rd = 0, \omega = 5$ with step-size 0.01.The obtained missing initial conditions $\left(F'(0), -G'(0), -\theta'(0)\right)$ are $a_1 = 1.9030, a_2 = 11.1405, a_3 = 0.9803$ by the Newton-Raphson iterative method the computed values are in relatively good agreements with [19] and [57]. Whereas, if we set $n = 1.3, M = L = \phi = Rd = 0, Pr = 1, \theta_w = 1, w = 1$, then with the Newton-Raphson method the values $a_1 = 0.5215, a_2 = 0.6033, a_3 = 0.3892$ are achieved for missing initial conditions $\left(F'(0), -G'(0), -\theta'(0)\right)$ where an excellent validity trend can be observed as mentioned in [22], [25], [26], and [27].

5. Convergence Analysis

Shooting is the most used numerical method because it is extremely effective in solving the complex differential systems of ODEs like the equations (32). It can also be employed because of its low computational cost and high level of accuracy as one can predict from the tables 2-10.

Table 2: Tabular comparison for $F'(0)$ when $n = \theta_w = Pr = 1,\ M = 0 = \Phi = Rd = a/c = 0$.

	ω	$F'(0)$		
		Present	Ref. [19]	Ref. [57]
M=0	0	-1.1737	−1.1737	−1.1737
	1	-0.9483	−0.9483	−0.9483
	2	-0.3262	−0.3263	−0.3262
	5	3.1937	3.1937	3.1937
	10	12.7206	12.7206	12.7209
	20	40.9056	40.9056	40.9057
M=2	0	1.8305	−1.8305	−1.8305
	1	-1.6634	−1.6635	−1.6634
	2	-1.1753	−1.1754	−1.1753
	5	1.8930	1.8928	1.8929
	10	10.8334	10.8329	10.8334
	20	38.1880	38.1857	38.1880

Table 3: Tabular comparison for $G'(0)$, when $n = \theta_w = Pr = 1,\ M = 0 = \Phi = Rd = a/c = 0$.

	ω	$-G'(0)$		
		Present	Ref. [19]	Ref. [57]
M=0	0	0.0000	0.0000	0.0000
	1	1.4870	1.4870	1.4870
	2	3.1278	3.1278	3.1278
	5	9.2535	9.2536	9.2535
	10	22.9132	22.9139	22.9134
	20	60.0126	59.6895	60.0129
M=2	0	0.0000	0.0000	0.0000
	1	2.0239	2.0239	2.0239
	2	4.1135	4.1135	4.1135
	5	11.1405	11.1407	11.1406
	10	25.7225	25.7231	25.7225
	20	64.0603	64.0635	64.0604

Table 4: Tabular comparison for $\theta'(0)$, when $n = \theta_w = Pr = 1,\ M = 0 = \Phi = Rd = a/c = 0$.

	ω	$-\theta'(0)$		
		Present	Ref. [19]	Ref. [57]
M=0	0	0.8520	0.8520	0.8520
	1	0.8757	0.8757	0.8757
	2	0.9304	0.9304	0.9304
	5	1.1291	1.1292	1.1291
	10	1.4260	1.4260	1.4259
	20	1.8944	1.8743	1.8944
M=2	0	0.7261	0.7261	0.7261
	1	0.7422	0.7422	0.7422
	2	0.7854	0.7854	0.7854
	5	0.9803	0.9803	0.9803
	10	1.2993	1.2993	1.2992
	20	1.7973	1.7974	1.7973

Table 5: Comparison of $F'(0)$, when $M = L = \phi = Rd = 0, Pr = 1, \theta_w = 1, w = 1$.

n	$F'(0)$				
	Present	Ref. [22]	Ref. [25]	Ref. [26]	Ref. [27]
2.5	0.5623	-	0.56236	-	0.5624
2.2	0.5531	-	0.55319	-	0.5532
2.0	0.5467	0.547	0.54676	-	0.5468
1.7	0.5366	0.537	0.53664	-	0.5366
1.5	0.5291	0.529	0.52919	0.526405	0.5292
1.3	0.5215	0.522	0.52150	0.519894	0.5215
1.1	0.5140	0.514	-	0.513389	-
1.0	0.5102	0.510	0.51021	0.510232	0.5102
0.9	0.5067	0.507	-	0.507189	-
0.8	0.5037	0.504	0.50381	0.504218	0.5038
0.6	0.5012	0.501	-	0.497596	-
0.5	0.5006	0.501	0.50058	0.493192	0.5006
0.2	0.5328	0.532	-	-	-

Table 6: Comparison of $-G'(0)$, when $M = L = \phi = Rd = 0, Pr = 1, \theta_w = 1, w = 1$.

n	$-G'(0)$				
	Present	Ref. [22]	Ref. [25]	Ref. [26]	Ref. [27]
2.5	0.6096	-	0.60967	-	0.6096
2.2	0.6075	-	0.60566	-	0.6057
2.0	0.6033	0.603	0.60327	-	0.6033
1.7	0.6009	0.600	0.60091	-	0.6009
1.5	0.6010	0.601	0.60099	0.613704	0.6010
1.3	0.6033	0.603	0.60346	0.612860	0.6035
1.1	0.6105	0.610	-	0.614173	-
1.0	0.6159	0.616	0.61591	0.615921	0.6159
0.9	0.6237	0.624	-	0.618427	-
0.8	0.6348	0.636	0.63608	0.621449	0.6361
0.6	0.6740	0.676	-	0.628137	-
0.5	0.7080	0.712	0.71322	0.632581	0.7130
0.2	1.0320	1.032	-	-	-

Table 7: Comparison of $-H(\infty)$, when $M = L = \phi = Rd = 0, Pr = 1, \theta_w = 1, w = 1$.

n	$-H'(\infty)$				
	Present	Ref. [22]	Ref. [25]	Ref. [26]	Ref. [27]
2.5	0.5425	-	0.54200	-	0.5425
2.2	0.5655	-	0.56553	-	0.5655
2.0	0.5877	0.586	0.58765	-	0.5877
1.7	0.6366	0.633	0.63662	-	0.6366
1.5	0.6783	0.676	0.67828	0.663515	0.6783
1.3	0.7359	0.735	0.73591	0.724913	0.7359
1.1	0.8101	0.822	-	0.817372	-
1.0	0.8823	0.883	0.88230	0.884473	0.8823
0.9	0.9694	0.969	-	0.975412	-
0.8	1.0594	1.089	1.05929	1.093999	1.0593
0.6	1.3641	1.364	-	1.360137	-
0.5	1.5437	1.539	1.54389	1.464609	1.5438
0.2	1.7788	-	-	-	-

Table 8: Comparison of the $\theta'(0)$, when $M = L = \phi = Rd = 0, Pr = 1, \theta_w = 1, w = 1$.

n	$\theta'(0)$		
	Present	Ref. [25]	Ref. [27]
2.5	0.3998	0.39980	0.3996
2.2	0.3966	0.39655	0.3965
2.0	0.3939	0.39392	0.3939
1.7	0.3896	0.38970	0.3897
1.5	0.3884	0.38859	0.3886
1.3	0.3892	0.38910	0.3891
1.1	0.3922	-	
1.0	0.3963	0.39632	0.3963
0.9	0.4024	-	-
0.8	0.4114	0.41108	0.4111
0.6	0.4501	-	-
0.5	0.4793	0.47917	0.4791
0.2	0.8226	-	-

It can be noticed that the results in tables 2-4 are in good agreement with Ref. [19] and Ref. [57] respectively. Similarly, tables 5-8 are extracted for velocity components and temperature profile to show the validation of code and our numerically approached technique more precisely by setting parameters as $M = L = \phi = Rd = 0, Pr = 1, \theta_w = 1, w = 1$ for various values of the power-law index n and an excellent level of accuracy can be observed with those which are illustrated in [22], [25], [26] and [27] respectively.

Table 9: Comparison for Skin friction coefficients when $n = 1, L = \phi = 0, Rd = 1, Pr = 1, \theta_w = 1, w = 1$.

M	$Re_r^{\frac{1}{n+1}} C_{Fr}$		$Re_r^{\frac{1}{n+1}} C_{G\theta^*}$	
	Present	Nabil T. [26]	Present	Nabil T. [26]
0	0.5102	0.510232	-0.6159	− 0.615921
0.5	0.3851	0.385132	-0.8487	− 0.848723
1	0.3092	0.309257	-1.0691	− 1.069053
2	0.2305	0.230559	-1.4421	− 1.442094
4	0.1657	0.165703	-2.0103	− 2.010266
Slp	**-0.07755**		**-0.34397**	

Table 10: Comparison of local Nusselt number when $n = 1,\ M = 1, L = \phi = 0, \theta_w = 1, w = 1$

Rd	$Pr = 0.72$		$P = 1$		$P = 7$	
	$Re_r^{-\frac{1}{n+1}} Nu_r$		$Re_r^{-\frac{1}{n+1}} Nu_r$		$Re_r^{-\frac{1}{n+1}} Nu_r$	
	Present	Nabil T. [26]	Present	Nabil T. [26]	Present	Nabil T. [26]
1	0.1562	0.1562525	0.1701	0.1701405	0.4559	0.4450890
3	0.1780	0.1780635	0.1995	0.1995045	0.6541	0.6541676
5	0.1858	0.1858858	0.2100	0.2100101	0.7328	0.7328291
10	0.1932	0.1932714	0.2199	0.2199356	0.8084	0.8084313
10^9	0.2025	0.2025129	0.2323	0.2323802	0.9045	0.9045440

Moreover, the skin friction in radial as well as in azimuthal directions and local Nusselt number for various values of the parameter of magnetic field M and radiation parameter Rd together with some particular values of Prandtl's number Pr are pondered in tables 9-10. The calculated values are correct up to 4 decimal places in comparison with that of [26]. Hence it can be observed that the shooting method is extremely effective for finding the solution to such types of highly nonlinear fluid flow problems. Also upon using the slope of the linear regression through data points as suggested by [58-60], it is worth remarking that the skin friction in radial direction decreases with higher Lorentz force at the rate of −0.07755. The outcome of the slope of the linear regression through data points shows that the skin

friction in radial azimuthal directions decreases with the parameter associated with the Lorentz force at the higher rate of −0.34397. Hence it is worth mentioning that the shooting method is extremely effective for finding the solution of such highly nonlinear fluid flow problems with a significant converging rate.

6. Results and discussion

In this portion of the analysis, the effects of several types of promising parameters are analyzed on the power-law ferrofluid in the presence of nonlinear thermally radiated MHD stagnation point flow on a rotatory stretchable disk and some physical quantities are also deliberated. The tabular comparison and graphical demonstration of outcomes is reflected with the aim of radial and azimuthal velocity components, temperature field, the radial and azimuthal directions skin friction coefficients, and local Nusselt number alongside the non-dimensional parameters that is volume fraction parameter ϕ, the parameter of magnetic field M, the rotation parameter ω, index of power-law n, the ratio of temperature θ_w, radiation parameter Rd, and Prandtl number Pr. A thorough discussion is constituted for Newtonian $n = 1$ and non-Newtonian which incorporates the shear-thinning $n < 1$ and shear-thickening $n > 1$ fluid.

4.1 Influence of volume fraction ϕ

The influence of the parameter of volume fraction ϕ on the radial F as well as azimuthal G velocities and temperature θ fields are depicted in figures 2-4 by assuming ferrite (Fe_3O_4) as ferrofluid particle which is composed of water as a base fluid and setting the other involved parameters as $Pr = 7, \mathrm{M} = 3, \mathrm{L} = 1.5, \mathrm{Rd} = 2, \theta_w = 1.3, \omega = 0.5$. Figure 2 shows the increasing behaviors for Newtonian and non-Newtonian fluids along the dimensionless similarity variable η. When the Ferro-particle magnetite is not operative $(i.e.\phi = 0)$ the value of radial velocity is maximum inside the boundary layer and with the rise in the parameter of volume fraction, it decreases for Newtonian and non-Newtonian fluids. Physically, it is because the viscosity of ferrofluid enhances as ϕ increases due to which the momentum diffusivity increases in the boundary layer. Also, an increase in the power-law index n the radial velocity, and the thickness of the boundary layer decreases. The upshots of the parameter of volume fraction on the azimuthal velocity in figure 3 shows an opposite trend as that of radial velocity in figure 2. Figure 4 indicates the temperature and the thermal thickness of the boundary layer are increasing by heightening the parameter of volume fraction along the similarity variable η. The temperature for shear-thinning $n < 1$ increased dramatically with that of Newtonian $n = 1$ and shear-thickening $n > 1$ fluid where the minor effects are noticed.

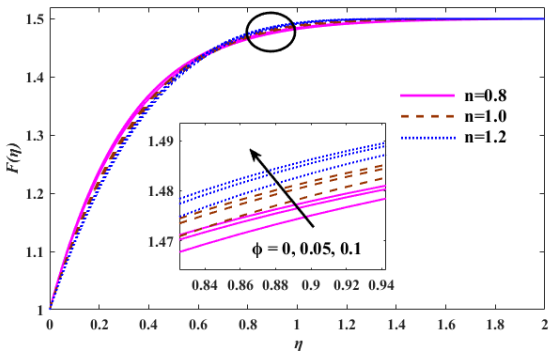

Fig. 2. Upshots of ϕ on radial velocity when $Pr = 7, M = 3, \lambda = 1.5, Rd = 2, \theta_w = 1.3, \omega = 0.5$.

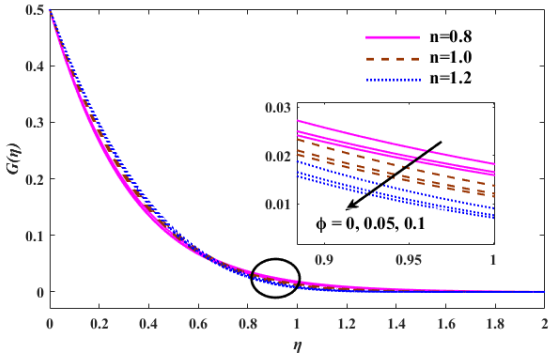

Fig. 3. Upshots of ϕ on azimuthal velocity when $Pr = 7, M = 3, \lambda = 1.5, Rd = 2, \theta_w = 1.3, \omega = 0.5$.

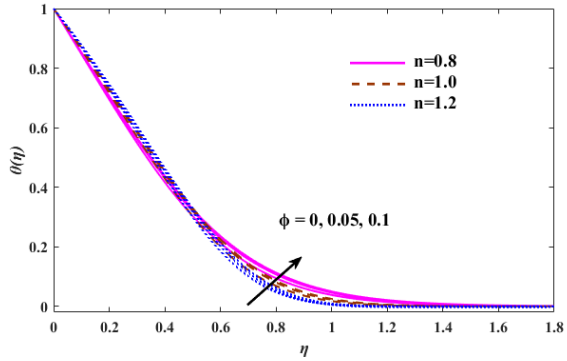

Fig. 4. Upshots of ϕ on temperature when $Pr = 7, M = 3,\ \lambda = 1.5, Rd = 2, \theta_w = 1.3, \omega = 0.5.$

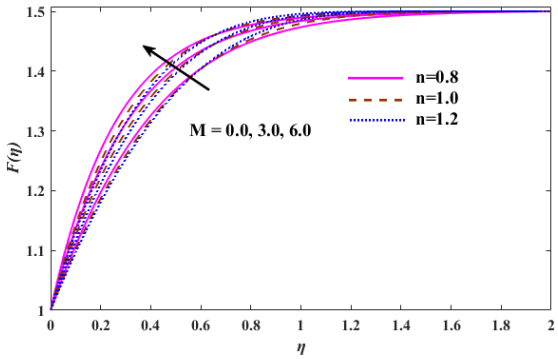

Fig. 5. Upshots of M on radial velocity when $Pr = 7, \phi = 0.05, \lambda = 1.5, Rd = 2,\ \theta_w = 1.3, \omega = 0.5.$

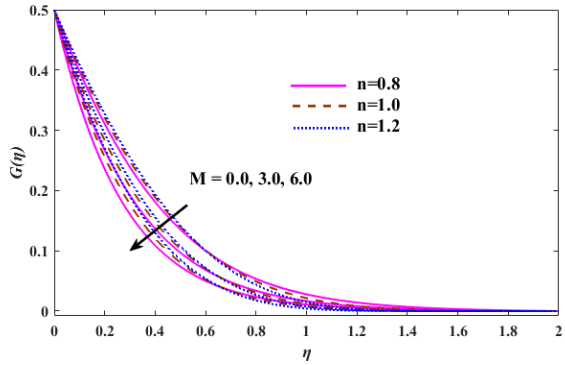

Fig. 6. Effect of M upon azimuthal velocity while $\mathrm{Pr} = 7, \phi = 0.05, \lambda = 1.5, \mathrm{Rd} = 2,\ \theta_w = 1.3, \omega = 0.5.$

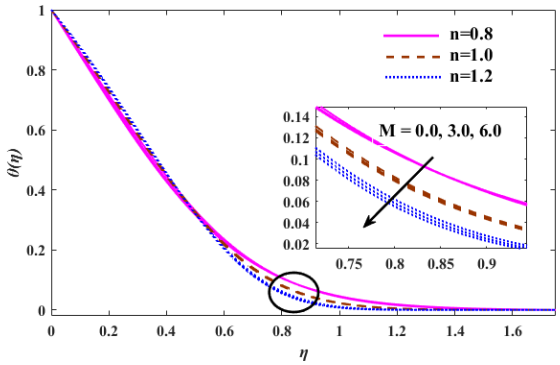

Fig. 7. Effect of M upon temperature while $Pr = 7, \phi = 0.05,\ \lambda = 1.5, Rd = 2, \theta_w = 1.3, \omega = 0.5.$

4.2 Influence of Magnetic parameter M

Figures 5-7 display that the escalation in magnetic parameter M causes a reduction in the radial F and azimuthal G velocities respectively, where the motion of axially rotating disk is drawn towards the surroundings of the surface for the compensation of radial outflow. It is obvious that raising the power-law index n the thickness of the boundary layer turned thinner. By the implementation of the magnetic field which refers to the similar effects of reducing the velocity with the consideration of various values of n which are stated for shear-thinning $(n < 1)$, Newtonian $n = 1$ and shear-thickening $n > 1$ fluids. Physically it is expressed as, the existence of Lorentz force which occurs due to the magnetic field that retards the flow near the disk. It can be reckoned that the boundary layer is thinner. Figure 7 signifies an increasing trend of temperature θ with the increasing magnetic parameter M for Newtonian and shear-thinning fluids. In the case of shear-thickening, the temperature is decreasing. Hence, the temperature inside the boundary layer reduces for shear-thickening fluids with a higher magnetic field.

4.3 Influence of rotation parameter ω

Figures 8-9 are drawn to show the effects of the rotation parameter ω upon radial as well as azimuthal velocities and temperature field. Figure 8 implies that the radial velocity escalates and by the rise in the parameter of rotation ω the thickness of the momentum boundary layer declines. Physically it can be interpreted as the particles of the ferrofluid are driven towards the radial direction because of the presence of centrifugal force due to which velocity increases. The increment in ω enhances the azimuthal component in figure 9 where the effects for shear-thickening fluid are more prominent.

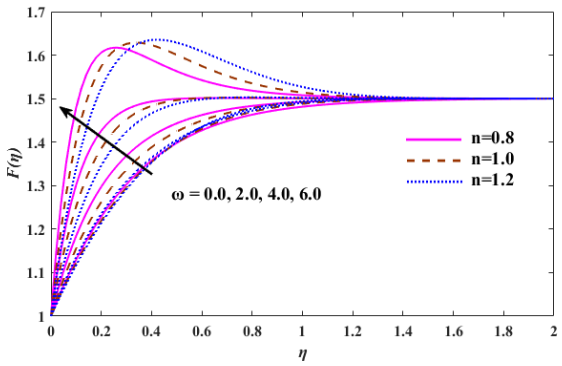

Fig. 8. Effect of ω on radial velocity while $Pr = 7, \phi = 0.05,\ \lambda = 1.5, Rd = 2, M = 3, \theta_w = 1.3.$

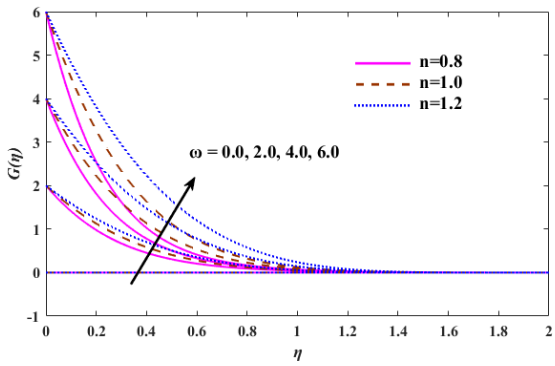

Fig. 9. Effect of ω on azimuthal velocity while $Pr = 7, \phi = 0.05,\ \lambda = 1.5, Rd = 2, M = 3, \theta_w = 1.3.$

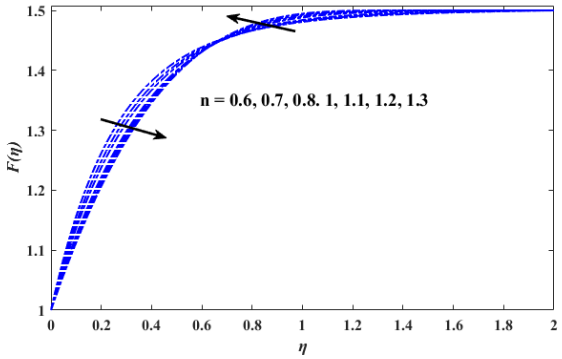

Fig. 10. Upshots of n on radial velocity when $Pr = 7, \phi = 0.05,\ \lambda = 1.5, Rd = 2, M = 3, \theta_w = 1.3,\ \omega = 0.5.$

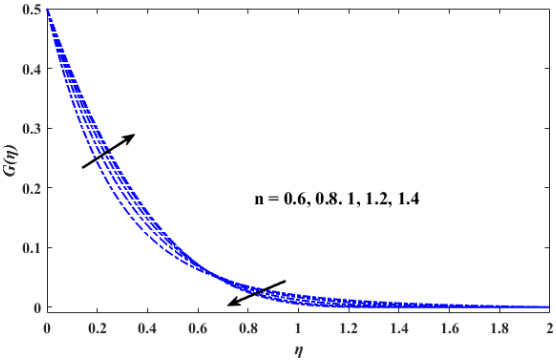

Fig. 11. Upshots of n on azimuthal velocity while $Pr = 7, \phi = 0.05,\ \lambda = 1.5, Rd = 2, M = 3, \theta_w = 1.3,\ \omega = 0.5.$

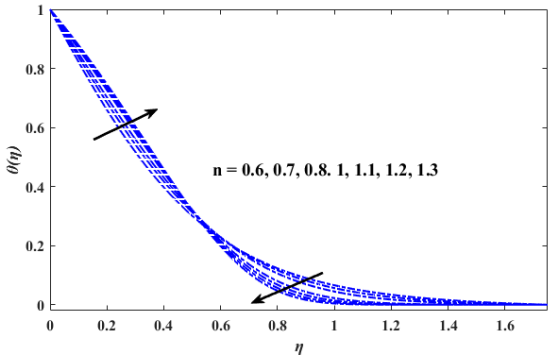

Fig. 12. Upshots of n on temperature when $Pr = 7, \phi = 0.05,\ \lambda = 1.5, Rd = 2, M = 3, \theta_w = 1.3,\ \omega = 0.5.$

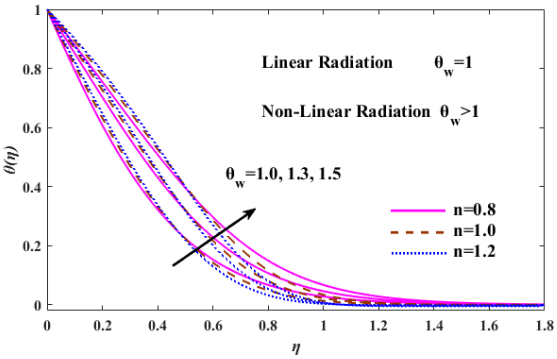

Fig. 13. Upshots of θ_w on temperature field when $Pr = 7, \phi = 0.05,\ \lambda = 1.5, Rd = 2, M = 3,\ \omega = 0.5.$

4.4 Influence of power-law index n

To show the influence of power-law index n upon the profiles of velocity and temperature figures 10-12 are drawn against the similarity variable η by setting other parameters as $Pr = 7, \phi = 0.05,\ \lambda = 1.5, Rd = 2, M = 3, \theta_w = 1.3,\ \omega = 0.5$. A cross-sectional type of flow is examined for the non-dimensional profiles of velocity and temperature. Also, the radial velocity in figure 10 is increasing near the wall whereas this trend gets reversed away from the wall. The azimuthal velocity in figure 11 is describing the opposite behavior from radial velocity in figure 11. A similar type of effect can be observed for the temperature field in figure 12. Hence, the thickness of the layer of boundary

declines by the upsurge in n. So, it can be concluded that the thickness of the boundary layer is thinner for shear-thickening and thicker for shear-thinning fluids. It is because of the increase in n which causes resistance near the disk.

4.5 Influence of linear and non-linear radiation

The effects of linear $\theta_w = 1$ and nonlinear radiations $\theta_w > 1$ on temperature θ profile for Newtonian $n = 1$ and non-Newtonian fluids $(n < 1, n > 1)$ by scaling other quantities as $Pr = 7, \phi = 0.05,\ \lambda = 1.5, Rd = 2, M = 3, \theta_w = 1.3, \omega = 0.5$ against η are analyzed in figure 13. Figure 13 differentiates the influence of linear and nonlinear radiation on temperature. It can be noted that with the enhancement in the temperature ration parameter θ_w which states the comparison between the larger wall temperature to that of ambient and consequently the temperature inflates. The effects of linear and nonlinear radiation are more distinguish for shear-thickening fluid $n > 1$ in comparison with Newtonian $n = 1$ and shear-thinning fluids $n < 1$. Nonlinear radiation increased the temperature of the fluid greatly. It can be concluded that the thickness of the boundary layer is increasing by the rise in θ_w but it reduces by increasing the n.

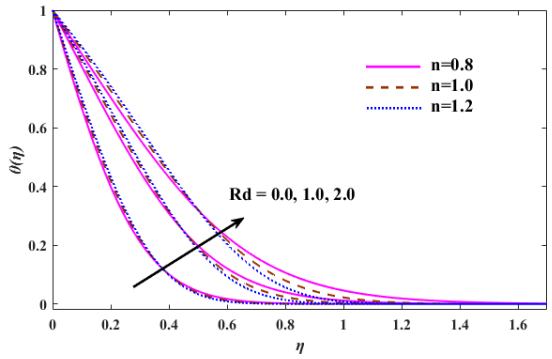

Fig. 14. Influence of Rd on temperature field when $Pr = 7, \phi = 0.05,\ \lambda = 1.5, M = 3, \theta_w = 1.3, \omega = 0.5$.

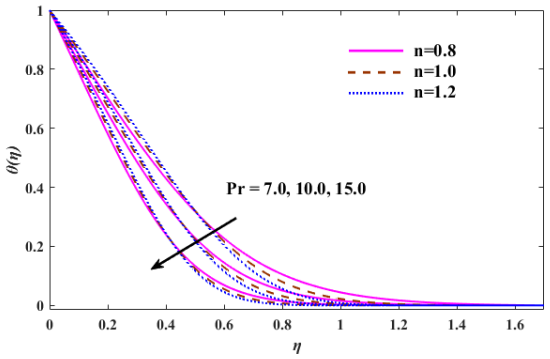

Fig. 15. Effect of Pr on temperature field while $\phi = 0.05,\ \lambda = 1.5, \mathrm{M} = 3, \mathrm{Rd} = 2, \theta_w = 1.3, \omega = 0.5$.

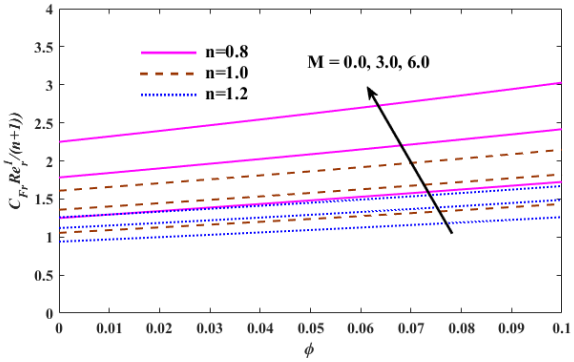

Fig. 16 Skin friction in the radial direction corresponding to ϕ when$M = 0, 3, 6\ \omega = 0.5, \lambda = 1.5, Pr = 7, Rd = 2, \theta_w = 1.3$.

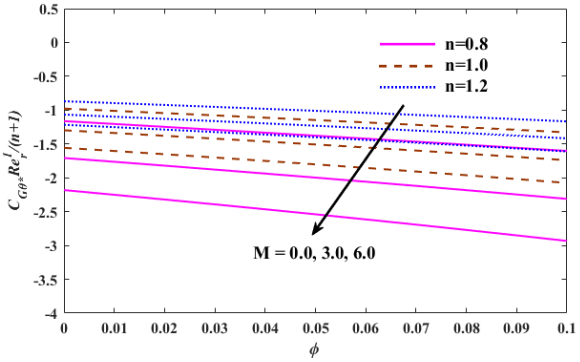

Fig. 17 Skin friction in the azimuthal direction corresponding to ϕ when $M = 0, 3, 6\ \omega = 0.5, \lambda = 1.5, Pr = 7, Rd = 2, \theta_w = 1.3$.

4.6 Influence of thermal radiation

Figure 14 asserted the upshots of the radiation parameter Rd upon the temperature θ for Newtonian and non-Newtonian fluids along the similarity variable η by assigning the values to the other involved quantities as $Pr = 7, \phi = 0.05,\ \lambda = 1.5, Rd = 2, M = 3,\ \omega = 0.5$. After the examination of figure 14, it can be predicted that the

behavior of the θ elevates. It can be physically expressed as by escalation within the radiation parameter the coefficient of mean absorption declines which delivers further heat towards the fluid because of which temperature enhances within the boundary layer. Hence, on enhancing Rd the boundary layer thickness is larger for shear-thinning fluid $n < 1$ than from shear-thickening fluid $n > 1$.

4.7 Influence of Prandtl number

The upshots of Prandtl number Pr upon temperature field θ are accentuated in figure 15. It can be witnessed that upon rising the Prandtl number it causes a reduction in the behavior of temperature because the Prandtl number associates the momentum and thermal diffusivities and by the enhancement in Prandtl number implies deduction within the thermal diffusivity because of this reason temperature decayed. The boundary layer reduces by escalating the Prandtl number for Newtonian and non-Newtonian fluids. The depletion in the boundary layer can be noticed slightly higher for shear-thickening fluid $(n > 1)$ than shear-thinning fluid $(n < 1)$.

4.8 Skin friction and local Nusselt number against volume fraction

The skin friction in radial $Re_r^{\frac{1}{n+1}} C_{Fr}$ as well as in azimuthal $Re_r^{\frac{1}{n+1}} C_{G\theta^*}$ directions and local Nusselt number $Re_r^{-\frac{1}{n+1}} Nu_r$ versus the parameter of volume fraction ϕ using different values of magnetic parameter M for Newtonian and non-Newtonian fluids are elucidated in the figures 16-18 under the consideration of magnetite (Fe_3O_4) as a ferrofluid particle and water as based fluid. Figure 16 explains that skin friction escalates in a radial direction. The concept behind this is that an increase in the parameter ϕ causes higher viscosity for ferrofluids which further enhances the concentration of magnetic nanoparticles within the base fluid. The influence of skin friction for shear-thinning fluid $n < 1$ is noticeable with the elevation in the magnetic parameter M in a comparison with Newtonian $n = 1$ and shear-thickening fluids $n > 1$. The consequences of skin friction in azimuthal direction elucidate the opposite trend to that which is described in figure 17. Figure 18 is reflecting two opposite behaviors for Nusselt number which is escalating along with the parameter of volume fraction ϕ for shear-thinning fluid $n < 1$ with the escalating magnetic parameter M, but with the rise in n the minor influences can be noticed for Newtonian fluid $n = 1$ also for shear-thinning fluid $n > 1$ the trend is decreasing.

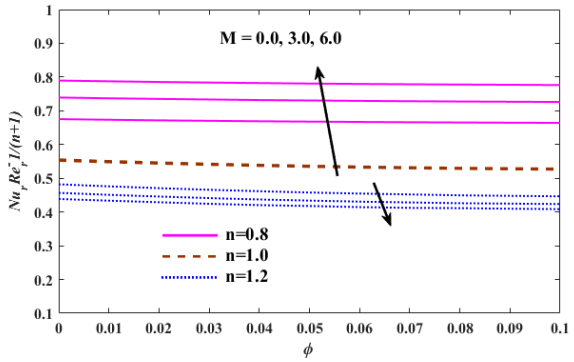

Fig. 18 Local Nusselt number corresponding to ϕ when $M = 0, 3, 6\ \omega = 0.5, \lambda = 1.5, Pr = 7, Rd = 2, \theta_w = 1.3$.

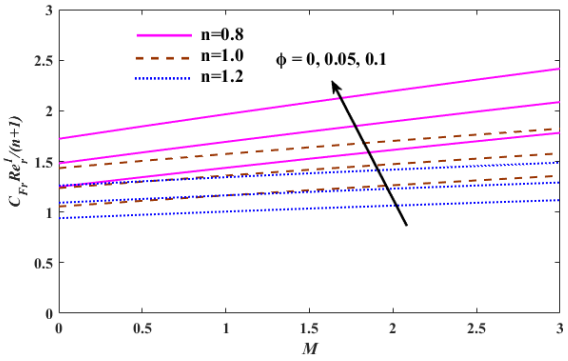

Fig. 19 Skin friction in the radial direction corresponding to M when $\phi = 0, 0.05, 0.1, \omega = 0.5, \lambda = 1.5, Pr = 7, Rd = 2, \theta_w = 1.3$.

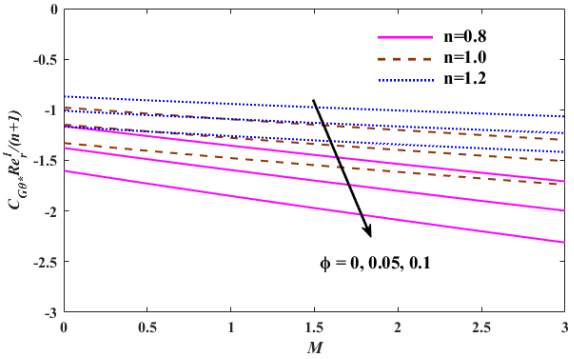

Fig. 20 Skin friction in the azimuthal direction corresponding to M when $\phi = 0, 0.05, 0.1, \omega = 0.5, \lambda = 1.5, Pr = 7, Rd = 2, \theta_w = 1.3$.

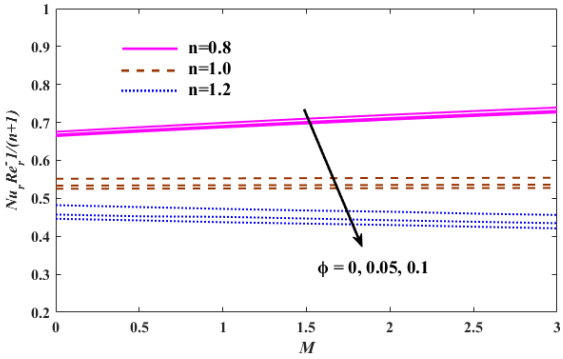

Fig. 21 Local Nusselt number against M when $\phi = 0, 0.05, 0.1, \omega = 0.5, \lambda = 1.5, Pr = 7, Rd = 2, \theta_w = 1.3$.

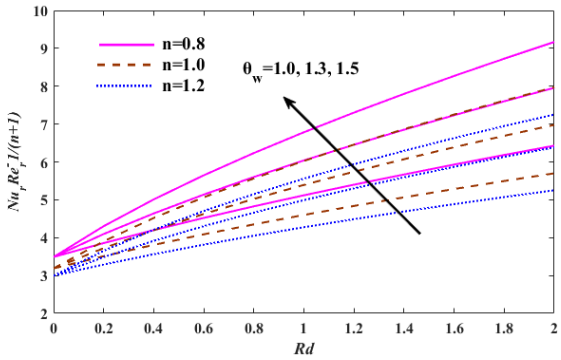

Fig. 23 Local Nusselt number against Rd when $\theta_w = 1, 1.3, 1.5, \omega = 0.5, M = 3, \phi = 0.05, \ \lambda = 1.5, Pr = 7$.

4.9 Skin friction and local Nusselt number against the magnetic parameter

Figures 19-21 explains the behavior of skin friction in radial $Re_r^{\frac{1}{n+1}} C_{Fr}$ as well as in azimuthal $Re_r^{\frac{1}{n+1}} C_{G\theta^*}$ directions and local Nusselt number $Re_r^{-\frac{1}{n+1}} Nu_r$ against the magnetic parameter M by boosting the parameter of volume fraction ϕ for Newtonian and non-Newtonian fluids. The skin friction in figure 19 is increasing along M with the escalation in ϕ. The larger effects can be regarded for shear-thinning fluid than Newtonian and shear-thickening fluids. From figures 20 and 21 a decreasing trend can be perceived for skin friction in the azimuthal direction and local Nusselt number by the rise in ϕ in the case of Newtonian and non-Newtonian fluids.

4.10 Local Nusselt number against the radiation parameter

The local Nusselt number $Re_r^{-\frac{1}{n+1}} Nu_r$ against the radiation parameter Rd in the case of linear $\theta_w = 1$ and nonlinear $\theta_w > 1$ radiations for Newtonian and non-Newtonian fluids by fixing the parameters as $\omega = 0.5, M = 3, \phi = 0.05, \lambda = 1.5, Pr = 7$ is plotted in figure 22. It can be demonstrated that the influence of radiation causes an increase in the behavior of $Re_r^{-\frac{1}{n+1}} Nu_r$ and this increase for nonlinear radiation is greater in comparison with that of linear radiation. The shear-thinning for linear and nonlinear radiation is larger from shear-thickening.

7. Conclusions

The steady three-dimensional flow of power-law fluid near the stagnation point and heat transfer within the boundary layer is investigated. A similarity solution of the water/magnetite nanofluid modeled partial differential equations subject to thermal radiation and Lorentz force over stretchable rotating disks is obtained. The influence of several emerging quantities upon the non-dimensional distributions of velocity and temperature for Newtonian and non-Newtonian shear-thinning and shear-thickening fluids are debated briefly in tabular and graphical forms. The physically interesting quantities are also determined and the effects are analyzed. From overall perspectives and explorations the following consequences can be drawn:

- Upon increasing the concentration of nano-particles the velocity components are in a similar trend.
- The rise in M causes the existence of Lorentz force which decreases the velocity components.
- The velocity components increase as the disk rotation rate increases.
- A cross-sectional flow is noticed for velocity and temperature profiles when the power-law index increases.
- Nonlinear radiation escalates the temperature than from linear radiation
- Temperature is augmenting for radiation parameters but decays for Prandtl number.
- The skin frictions coefficients are in opposite behavior along ϕ for diverse M.
- The local Nusselt number plummets against M for various ϕ but augments along Rd for different θ_w.

References

[1] S.U.S. Choi, Enhancing thermal conductivity of fluids with nanoparticles, Proc. Int. Mech. Eng. Congress. San Francisco, USA, ASME, FED 231/MD 66 1995, pp. 99–105.

[2] E. Abu-Nada, Application of nanofluids for heat transfer enhancement of separated flows encountered in a backward-facing step, Int. J. Heat Fluid Flow 29 (2008) 242–249.

[3] R.J. Tiwari, M.K. Das, Heat transfer augmentation in a two-sided lid-driven differentially heated square cavity utilizing nanofluids, Int. J. Heat Mass Transf. 50 (2007) 2002–2018.

[4] Y. Jaluria, O. Manca, D. Poulikakos, K. Vafai, L. Wang, Heat transfer in nanofluid, Adv. Mech. Eng. 1–2 (2012), 972973.

[5] N. Bachok, A. Ishak, R. Nazar, I. Pop, Flow and heat transfer at a general three-dimensional stagnation point in a nanofluid, Phys. B 405 (2010) 4914–4918.

[6] M. JayachandraBabu, N.Sandeep. 3D MHD slip flow of a nanofluid over a slendering stretching sheet with thermophoresis and Brownian motion effects. Journal of Molecular Liquids. 222 (2016) 1003-1009. https://doi.org/10.1016/j.molliq.2016.08.005.

[7] Mustafa M, Mushtaq A, Hayat T, Alsaedi A (2016) Rotating Flow of Magnetite-Water Nanofluid over a Stretching Surface Inspired by Non-Linear Thermal Radiation. PLoS ONE 11(2): e0149304. https://doi.org/10.1371/journal.pone.0149304.

[8] Anu, K., & Hemalatha, J. (2016). Viscosity studies of water-based magnetite nanofluids. AIP Conference Proceedings 1731, 050148 (2016) http://dx.doi.org/10.1063/1.4947802.

[9] Amini, M., GhasemiKafrudi, E., Habibi, M. R., Ahmadi, A., & HosseinNia, A. (2017). MHD flow and heat transfer of a magnetite–water nanofluid in porous medium under the effects of chemical reaction. World Journal of Engineering, 14(3), 193–199. https://doi.org/10.1108/wje-07-2016-0020.

[10] Hayat, T., Rashid, M., & Alsaedi, A. (2018). Three-dimensional radiative flow of magnetite-nanofluid with homogeneous-heterogeneous reactions. Results in Physics, 8, 268–275. https://doi.org/10.1016/j.rinp.2017.11.038.

[11] Bhatti, M. M., Khalique, C. M., Bég, T. A., Bég, O. A., & Kadir, A. (2019). Numerical study of slip and radiative effects on magnetic Fe3O4water-based nanofluid flow from a nonlinear stretching sheet in porous media with Soret and Dufour diffusion. Modern Physics Letters B, 2050026. https://doi.org/10.1142/s0217984920500268.

[12] M. Zaydan, A. Wakif, I.L. Animasaun, U. Khan, D. Baleanu, R. Sehaqui, Significances of Blowing and Suction Processes on the Occurrence of Thermo-Magneto-Convection Phenomenon in a Narrow Nanofluidic Medium: A Revised Buongiorno's Nanofluid Model, Case Studies in Thermal Engineering, https://doi.org/10.1016/j.csite.2020.100726.

[13] Wakif A., Animasaun I. L., Satya Narayana P. V., Sarojamma G., Meta-analysis on thermo-migration of tiny/nano-sized particles in the motion of various fluids, Chinese Journal of Physics (2019), https://doi.org/10.1016/j.cjph.2019.12.002.

[14] Nehad Ali Shah1, L Animasaun, Abderrahim Wakif, O K Koriko, R Sivaraj, KS Adegbie, Zahra Abdelmalek, H Vaidyaa, A F Ijirimoye, and K V Prasad. Significance of suction and dual stretching on the dynamics of various hybrid nanofluids: Comparative analysis between type I and type II models. Phys. Scr. 95 (2020) 095205 (14pp) https://doi.org/10.1088/1402-4896/aba8c6.

[15] Kármán TV (1921) Über laminare und turbulente Reibung. Z Angew Math Mech 1:233–252. https://doi.org/10.1002/zamm.19210 01040 1.

[16] W.G. Cochran, S. Goldstein, The flow due to a rotating disk, Mathematical Proceedings of the Cambridge Philosophical Society 30 (3) (1934) 365–375.

[17] M.H. Rogers, G.N. Lance, The rotationally symmetric flow of a viscous fluid in the presence of an infinite rotating disk, Journal of Fluid Mechanics 7 (1960) 617–631.

[18] M. Turkyilmazoglu, Exact solutions corresponding to the viscous incompressible and conducting fluid flow due to a porous rotating disk, J. Heat Transfer 131, 091701 (2009).

[19] Irfan Mustafa, Tariq Javed, Abuzar Ghaffari, Heat transfer in MHD stagnation point flow of a ferrofluid over a stretchable rotating disk, Journal of Molecular Liquids 219 (2016) 526–532.

[20] P. Mitschka, Nicht-Newtonsche Flüssigkeiten II. Drehstromungen Ostwald-de Waelescher Nicht-Newtonscher Flüssigkeiten, Collection of Czechoslovak Chemical Communications 29 (1964) 2892–2905.

[21] P. Mitschka, and Ulbricht, J. 1965 Collect. Czech. Chem. Commun. 30, 2511.

[22] H. I. Andersson, E. De Korte, E., and R. Meland, 2001 Flow of a Power-Law Fluid over a Rotating Disk Revisited. Fluid Dynamics Research. 28, 75-88.

[23] H.I. Andersson, E. de Korte, MHD flow of a power-law fluid over a rotating disk, European Journal of Mechanics B/Fluids 21 (2002) 317–324.

[24] Lian-Cun, Z., Xin-Xin, Z., & Lian-Xi, M. (2008). Fully Developed Convective Heat Transfer of Power-Law Fluids in a Circular Tube. Chinese Physics Letters, 25(1), 195–197. https://doi.org/10.1088/0256-307x/25/1/053.

[25] Chunying Ming, Liancun Zheng and Xinxin Zhang, Steady flow and heat transfer of the power-law fluid over a rotating disk, International Communications in Heat and Mass Transfer 38 (2011) 280–284.

[26] Nabil T. EL-Dabe, Hazim A. Attia, Mohamed A. I. Essawy, Ibrahim H. Abd-elmaksoud, Ahmed A. Ramadan, Alaa H. Abdel-Hamid, Nonlinear heat and mass transfer in a thermal radiated MHD flow of a power-law nanofluid over a rotating disk, SN Applied Sciences (2019) 1:551 https://doi.org/10.1007/s42452-019-0557-6.

[27] Usman, Lin, P. & Ghaffari, A. Steady flow and heat transfer of the power-law fluid between two stretchable rotating disks with non-uniform heat source/sink. J Therm Anal Calorim (2020). https://doi.org/10.1007/s10973-020-10142-x.

[28] Lai, M.-C. (2001). A note on finite difference discretizations for Poisson equation on a disk. Numerical Methods for Partial Differential Equations, 17(3), 199–203. https://doi.org/10.1002/num.1.

[29] Dinarvand, S., Rashidi, M. M., & Shahmohamadi, H. (2009). Analytic approximate solution of three-dimensional Navier-Stokes equations of flow between two stretchable disks. Numerical Methods for Partial Differential Equations, NA–NA. https://doi.org/10.1002/num.20514.

[30] Shahzad, F., Hayat, T., Ayub, M., & Asghar, S. (2010). Unsteady MHD flow due to noncoaxial rotations of micropolar fluid and an accelerated disk with partial slip condition. Numerical Methods for Partial Differential Equations, 26(1), 176–187. https://doi.org/10.1002/num.20424.

[31] Rashidi, M. M., Shahmohamadi, H., & Domairry, G. (2011). Variational iteration method for solving three-dimensional Navier-Stokes equations of flow between two stretchable disks. Numerical Methods for Partial Differential Equations, 27(2), 292–301. https://doi.org/10.1002/num.20522.

[32] T. Hayat, M.I. Khan, M. Farooq, A. Alsaedi, T. YasmeenImpact of Marangoni convection in the flow of carbon-water nanofluid with thermal radiation Int J Heat Mass Transf, 106 (2017), pp. 810-815.

[33] Y. Lin, L. Zheng, X. Zhang. Radiation effects on Marangoni convection flow and heat transfer in pseudo-plastic non-Newtonian nanofluids with variable thermal conductivity Int J Heat Mass Transf, 77 (2014), pp. 708-716.

[34] A. Mushtaq, M. Mustafa, T. Hayat, A. Alsaedi. Numerical study of the non-linear radiation heat transfer problem for the flow of a second-grade fluid Bulg Chem Commun, 47 (2015), pp. 725-732.

[35] Abderrahim Wakif. A Novel Numerical Procedure for Simulating Steady MHD Convective Flows of Radiative Casson Fluids over a Horizontal Stretching Sheet with Irregular Geometry under the Combined Influence of Temperature-Dependent Viscosity and Thermal Conductivity. Mathematical Problems in Engineering Volume 2020, Article ID 1675350, 20 pages https://doi.org/10.1155/2020/1675350.

[36] Wakif, A., Chamkha, A., Thumma, T., Animasaun, I. L., & Sehaqui, R. (2020). Thermal radiation and surface roughness effects on the thermo-magneto-hydrodynamic stability of alumina–copper oxide hybrid nanofluids utilizing the generalized Buongiorno's nanofluid model. Journal of Thermal Analysis and Calorimetry. https://doi.org/10.1007/s10973-020-09488-z.

[37] Wakif, A., Boulahia, Z., Ali, F., Eid, M. R., & Sehaqui, R. (2018). Numerical Analysis of the Unsteady Natural Convection MHD Couette Nanofluid Flow in the Presence of Thermal Radiation Using Single and Two-Phase Nanofluid Models for Cu–Water Nanofluids. International Journal of Applied and Computational Mathematics, 4(3). https://doi.org/10.1007/s40819-018-0513-y.

[38] C. Zhang, L. Zheng, X. Zhang, G. Chen. MHD flow and radiation heat transfer of nanofluids in porous media with variable surface heat flux and chemical reaction Appl Math Model, 39 (2015), pp. 165-181.

[39] Sravanthi, C. S. (2019). Effect of nonlinear thermal radiation on silver and copper water nanofluid flow due to a rotating disk with variable thickness in the presence of nonuniform heat source/sink using the homotopy analysis method. Heat Transfer-Asian Research. https://doi.org/10.1002/htj.21581.

[40] Waqas, H., Khan, S. U., Shehzad, S. A., & Imran, M. (2019). Significance of the nonlinear radiative flow of micropolar nanoparticles over porous surface with a gyrotactic microorganism, activation energy, and Nield's condition. Heat Transfer-Asian Research. https://doi.org/10.1002/htj.21539.

[41] Mkhatshwa, M. P., Motsa, S. S., & Sibanda, P. (2020). MHD mixed convective radiative flow of Eyring-Powell fluid over an oscillatory stretching sheet using bivariate spectral method on overlapping grids. Heat Transfer. https://doi.org/10.1002/htj.21898.

[42] H. Alfven, Existence of electromagnetic-hydrodynamic waves. Nature Publishing Group 150 (3805) (1942), 405–406. https://doi.org/10.1038/150405d0.

[43] Makinde, O. D., Sandeep, N., Ajayi, T. M., & Animasaun, I. L. (2018). Numerical Exploration of Heat Transfer and Lorentz Force Effects on the Flow of MHD Casson Fluid over an Upper Horizontal Surface of a Thermally Stratified Melting Surface of a Paraboloid of Revolution. International Journal of Nonlinear Sciences and Numerical Simulation, 19(2), 93–106. https://doi.org/10.1515/ijnsns-2016-0087.

[44] Animasaun, D. I. L., Mahanthesh, B., Jagun, A. O., Bankole, T. D., R, S., Shah, N. A., & Saleem, S. (2018). Influence of Lorentz force on the flow of 29nm CuO-Water nanofluid over an upper horizontal surface of a paraboloid of revolution: The case of Heat Transfer. Journal of Heat Transfer. https://doi.org/10.1115/1.4041971.

[45] Koriko, O.K., Adegbie, K.S., Animasaun, I.L. et al. Comparative Analysis Between Three-Dimensional Flow of Water Conveying Alumina Nanoparticles and Water Conveying Alumina–Iron(III) Oxide Nanoparticles in the Presence of Lorentz Force. Arab J Sci Eng 45, 455–464 (2020). https://doi.org/10.1007/s13369-019-04223-9.

[46] Mahanthesh, B., Lorenzini, G., Oudina, F. M., & Animasaun, I. L. (2019). Significance of exponential space- and thermal-dependent heat source effects on nanofluid flow due to radially elongated disk with Coriolis and Lorentz forces. Journal of Thermal Analysis and Calorimetry. https://doi.org/10.1007/s10973-019-08985-0.

[47] Li, Y., Yan, H., Massoudi, M., & Wu, W.-T. (2017). Effects of Anisotropic Thermal Conductivity and Lorentz Force on the Flow and Heat Transfer of a Ferro-Nanofluid in a Magnetic Field. Energies, 10(7), 1065. https://doi.org/10.3390/en10071065.

[48] Wakif, A., Qasim, M., Afridi, M. I., Saleem, S., & Al-Qarni, M. M. (2019). Numerical Examination of the Entropic Energy Harvesting in a Magnetohydrodynamic Dissipative Flow of Stokes' Second Problem: Utilization of the Gear-Generalized Differential Quadrature Method. Journal of Non-Equilibrium Thermodynamics, 0(0). https://doi.org/10.1515/jnet-2018-0099.

[49] Wakif, A., Chamkha, A., Animasaun, I. L., Zaydan, M., Waqas, H., & Sehaqui, R. (2020). Novel Physical Insights into the Thermodynamic Irreversibilities Within Dissipative EMHD Fluid Flows Past over a Moving Horizontal Riga Plate in the Coexistence of Wall Suction and Joule Heating Effects: A Comprehensive Numerical Investigation. Arabian Journal for Science and Engineering. https://doi.org/10.1007/s13369-020-04757-3.

[50] P. Ram, A. Bhandari, K. Sharma, Axi-symmetric ferrofluid flow with rotating disk in a porous medium, Int. J. Fluid Mech. 2 (2010) 151–161.

[51] P. Ram, K. Sharma, A. Bhandari, Effect of porosity on ferrofluid flow with rotating disk, Int. J. Appl. Math. Mech. 6 (2010) 67–76.

[52] P. Ram, K. Sharma, A. Bhandari, Effect of porosity on revolving ferrofluid flow with rotating disk, Int. J. Fluids Eng. 3 (2011) 261–271.

[53] Tasawar Hayat, Maria Imtiaz, Ahmed Alsaedi, Faris Alzahrani, Effects of homogeneous–heterogeneous reactions in flow of magnetite-(Fe_3O_4) nanoparticles by a rotating disk, Journal of Molecular Liquids 216 (2016) 845–855.

[54] P. Ram, K. Sharma. On the revolving ferrofluid flow due to rotating disk, Int. J. Nonlinear Sci. 13 (2012) 317–324.

[55] P. Ram, K. Sharma, Effect of rotation and MHD viscosity on ferrofluid flow with rotating disk, Indian J. Pure Appl. Phys. 52 (2014) 87–92.

[56] Mohsan Hassan, C. Fetecau, Aaqib Majeed, Ahmad Zeeshan, Effects of iron nanoparticles' shape on convective flow of ferrofluid under highly oscillating magnetic field over stretchable rotating disk, Journal of Magnetism and Magnetic Materials, 465 (2018) 531-539.

[57] M. Turkyilmazoglu. MHD fluid flow and heat transfer due to a stretching rotating disk, Int. J. Therm. Sci. 51(2012) 195–201. https://doi.org/10.1016/j.ijthermalsci.2011.08.016.

[58] Shah, N. A., Animasaun, I. L., Ibraheem, R. O., Babatunde, H. A., Sandeep, N., & Pop, I. (2018). Scrutinization of the effects of Grashof number on the flow of different fluids driven by convection over various surfaces. Journal of Molecular Liquids, 249, 980–990. https://doi.org/10.1016/j.molliq.2017.11.042.

[59] Wakif A., Animasaun I. L., Satya Narayana P. V., Sarojamma G., Meta-analysis on thermo-migration of tiny/nano-sized particles in the motion of various fluids, Chinese Journal of Physics (2019), https://doi.org/10.1016/j.cjph.2019.12.002.

[60] Animasaun, I. L., Ibraheem, R. O., Mahanthesh, B., & Babatunde, H. A. (2019). A meta-analysis on the effects of haphazard motion of tiny/nano-sized particles on the dynamics and other physical properties of some fluids. Chinese Journal of Physics. https://doi.org/10.1016/j.cjph.2019.06.007.